Solvent Quality and Nonbiological Oligomer Folding: Revisiting Conventional Paradigms Supplementary Information

Cedrix J. Dongmo Foumthuim,*,†,‡ Tobia Arcangeli,†,¶ Tatjana Škrbić,† and Achille Giacometti*,†,§

†*Dipartimento di Scienze Molecolari e Nanosistemi, Università Ca' Foscari Venezia, Via Torino 155, 30172, Mestre, Venezia, Italy*

‡*INFN, Sezione di Roma Tor Vergata, Via della Ricerca Scientifica 1, 00133 Roma, Italy*

¶*Dipartimento di Chimica, Materiali e Ingegneria Chimica "Giulio Natta", Politecnico di Milano, Sede Leonardo Edificio 6, Piazza Leonardo da Vinci 32, I-20133 Milano, Italy*

§*European Centre for Living Technology (ECLT) Ca' Bottacin, Dorsoduro 3911, Calle Crosera 30123 Venice, Italy*

E-mail: cedrix85@gmail.com,cedrix.dongmo@unive.it; achille@unive.it

Table SI: Solvent characteristics.

Solvents	Dielectric constants ϵ	Characteristic length Å
Water H_2O	80.04	1.515
Acetonitrile MeCN	37.5	3.00
Chloroform $CHCl_3$	4.81	2.56
Cyclohexane cC_6H_{12}	2.02	5.80
n-hexane nC_6H_{14}	1.88	6.34

Table SII: Enthalpic and entropic contributions to the solvation free energies ($kJ\,mol^{-1}$) for different polymer length *12mer*, *16mer*, and *20mer* in the three solvents used water H_2O, cyclohexane cC_6H_{12} and n-hexane nC_6H_{14} at 25°C.

Solvent	Oligomer	ΔG	ΔH	$-T\Delta S$
H_2O	12mer	-2751.16 ± 2.53	-3317.34 ± 1.40	566.18 ± 15.96
	16mer	-3766.96 ± 1.87	-4474.23 ± 4.44	707.27 ± 21.97
	20mer	-4714.84 ± 2.47	-5583.89 ± 5.52	869.05 ± 28.24
nC_6H_{14}	12mer	-2834.90 ± 1.65	-3495.28 ± 7.39	660.38 ± 20.69
	16mer	-3860.16 ± 3.17	-4691.91 ± 10.92	831.75 ± 24.30
	20mer	-4821.46 ± 1.26	-5962.94 ± 14.37	1141.47 ± 32.59
cC_6H_{12}	12mer	-2047.25 ± 3.62	-2093.73 ± 12.39	46.47 ± 29.71
	16mer	-2796.44 ± 4.17	-2957.97 ± 17.52	161.54 ± 35.30
	20mer	-3484.41 ± 2.44	-3739.65 ± 31.86	255.24 ± 50.83

Table SIII: Enthalpic and entropic contributions to the transfer free energies ($kJ\,mol^{-1}$) from water H_2O to cyclohexane cC_6H_{12} and from water H_2O to n-hexane nC_6H_{14} for different polymer lenght investigated here at 25°C.

	Oligomers	$\Delta\Delta G$	$\Delta\Delta H$	$-T\Delta\Delta S$
$\Delta\Delta G_{w>h}$	12mer	-83.74 ± 4.18	-177.94 ± 8.79	94.2 ± 36.65
	16mer	-93.2 ± 5.04	-217.68 ± 15.36	124.48 ± 46.27
	20mer	-106.62 ± 3.73	-379.05±19.89	272.42 ± 60.83
$\Delta\Delta G_{w>c}$	12mer	703.91 ± 6.15	1223.61 ± 13.79	-519.71 ± 45.67
	16mer	970.52 ± 6.04	1516.26 ± 21.96	-545.74 ± 57.27
	20mer	1230.43 ± 4.91	1844.24 ± 37.38	-613.81 ± 79.07

Table SIV: Fitting coefficients, a, b and c used to compute the hydration thermodynamics parameters along with their Pearson's correlation coefficients R^2.

Solvents	Oligomers	a	b	c	R^2
H_2O	12mer	-3771.02341	12.09052	-1.52167	0.97694
	16mer	-2323.17397	-45.94891	-45.94891	0.99460
	20mer	-5233.94976	-4.94615	1.17369	0.99770
nC_6H_{14}	12mer	-5036.00406	36.82547	-5.16760	0.99135
	16mer	-2547.90165	-45.37304	7.19105	0.99273
	20mer	-5833.73501	0.92616	0.43334	0.98644
cC_6H_{12}	12mer	-1103.28532	-22.09331	3.32196	0.83359
	16mer	-4239.92131	29.33924	-4.29966	0.86636
	20mer	-755.54073	-66.17863	10.00877	0.87533

Table SV: Summary of the slopes, intercepts to origin, and correlation coefficients for the linear fitting curves $-T\Delta S = f(\Delta H)$ a.k.a enthalpy-entropy compensation in water H_2O, cyclohexane cC_6H_{12} and n-hexane cC_6H_{12} for pPA and polyPHE.

Oligomers	Solvents	Slopes	Intercepts origin	Correlation coefficients
pPA	H_2O	-0.13354	118.76581	0.99868
	cC_6H_{12}	-0.12695	-217.61118	0.99955
	nC_6H_{14}	-0.19546	-44.07187	0.98920
polyPHE	H_2O	-0.74689	-151.72571	0.99185
	cC_6H_{12}	-0.10883	97.25740	0.94718

RDF

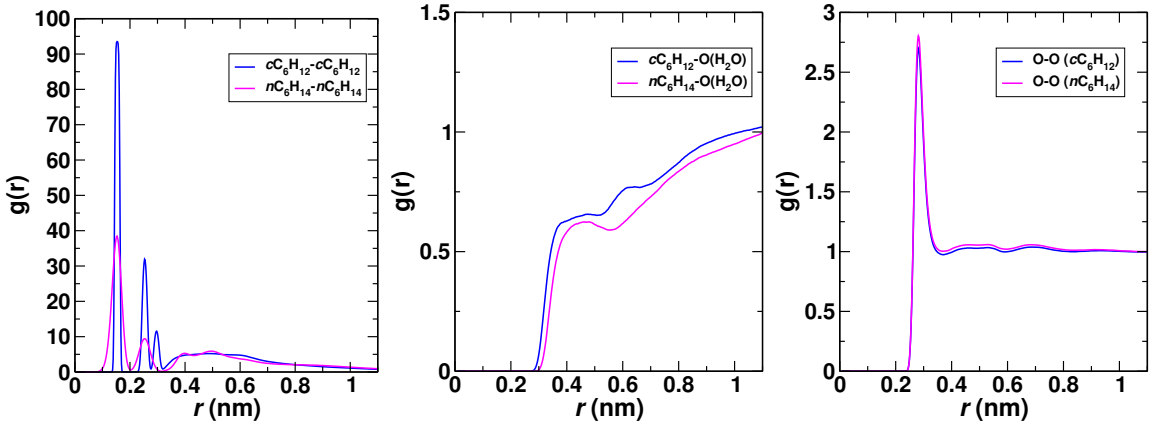

Figure SI: Site-site pair radial distribution functions computed for solute - solute (left), solute - water oxygen (middle), and water oxygen - water oxygen (right). cC_6H_{12} data are displayed in magenta while nC_6H_{14} counterparts are shown in blue.

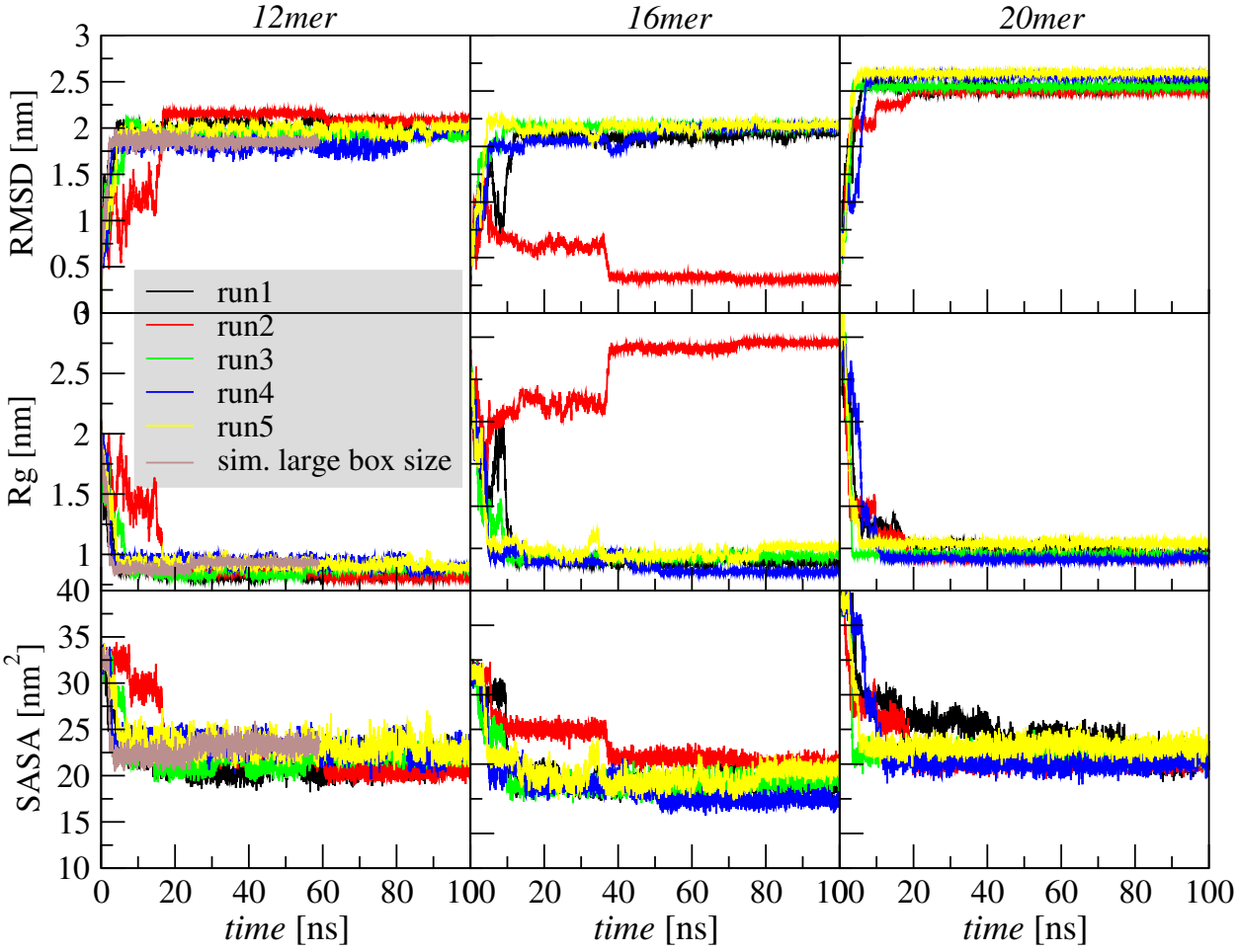

Figure SII: Folding trajectories of the pPA in water H_2O. From top to bottom the time-dependent changes of the RMSD, Rg and SASA are displayed, respectively. From left to right the changes in *12mer*, *16mer* and *20mer* oligomers are respectively shown.

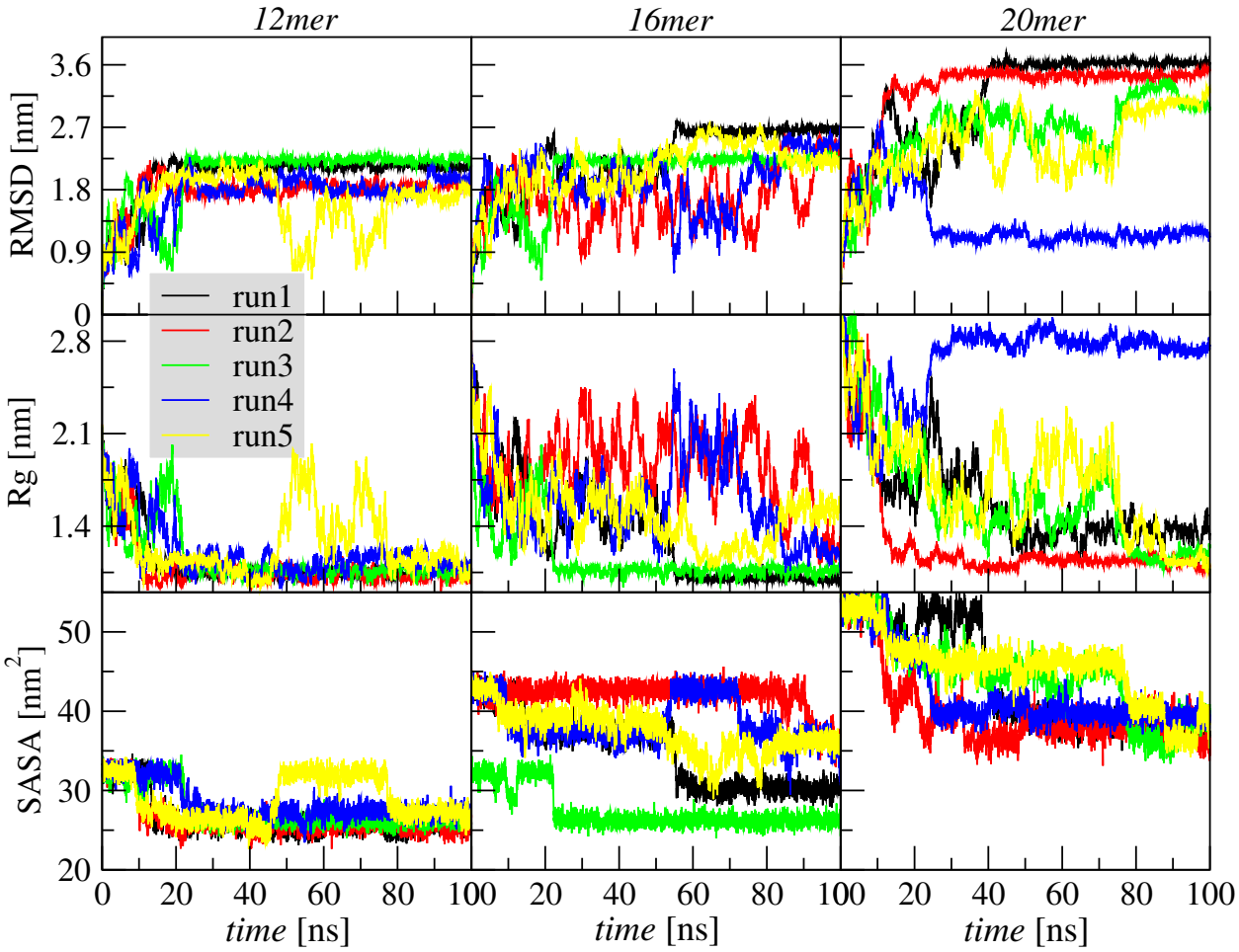

Figure SIII: Folding trajectories of pPA in cyclohexane cC_6H_{12}. From top to bottom the time-dependent changes of the RMSD, Rg and SASA are displayed, respectively. From left to right the changes in the oligomer length *12mer*, *16mer* and *20mer* are respectively shown.

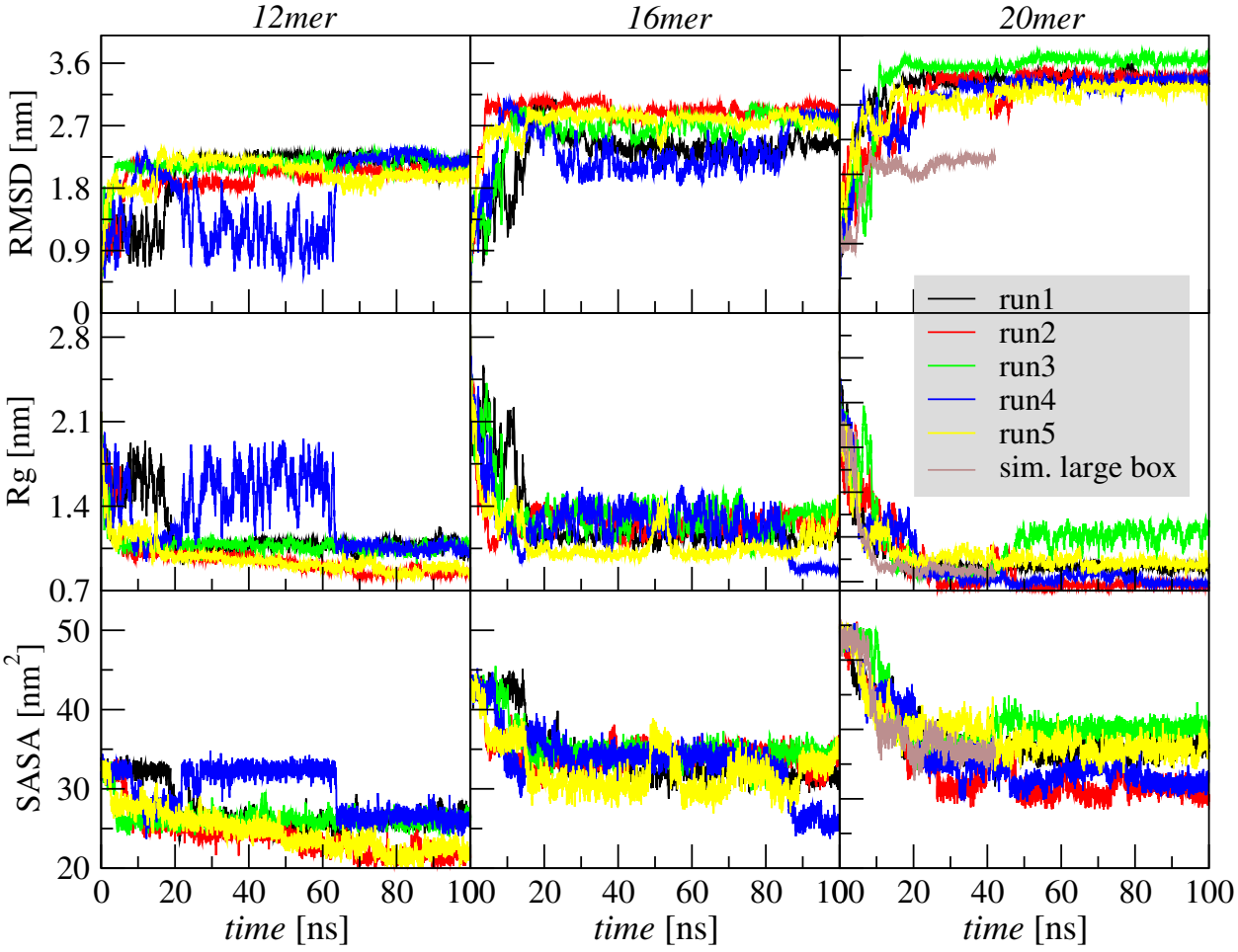

Figure SIV: Folding trajectories of pPA in *n*-hexane nC_6H_{14}. From top to bottom the time-based changes of the RMSD, Rg and SASA are displayed, respectively. From left to right the changes in oligomer length *12mer*, *16mer* and *20mer* are respectively shown.

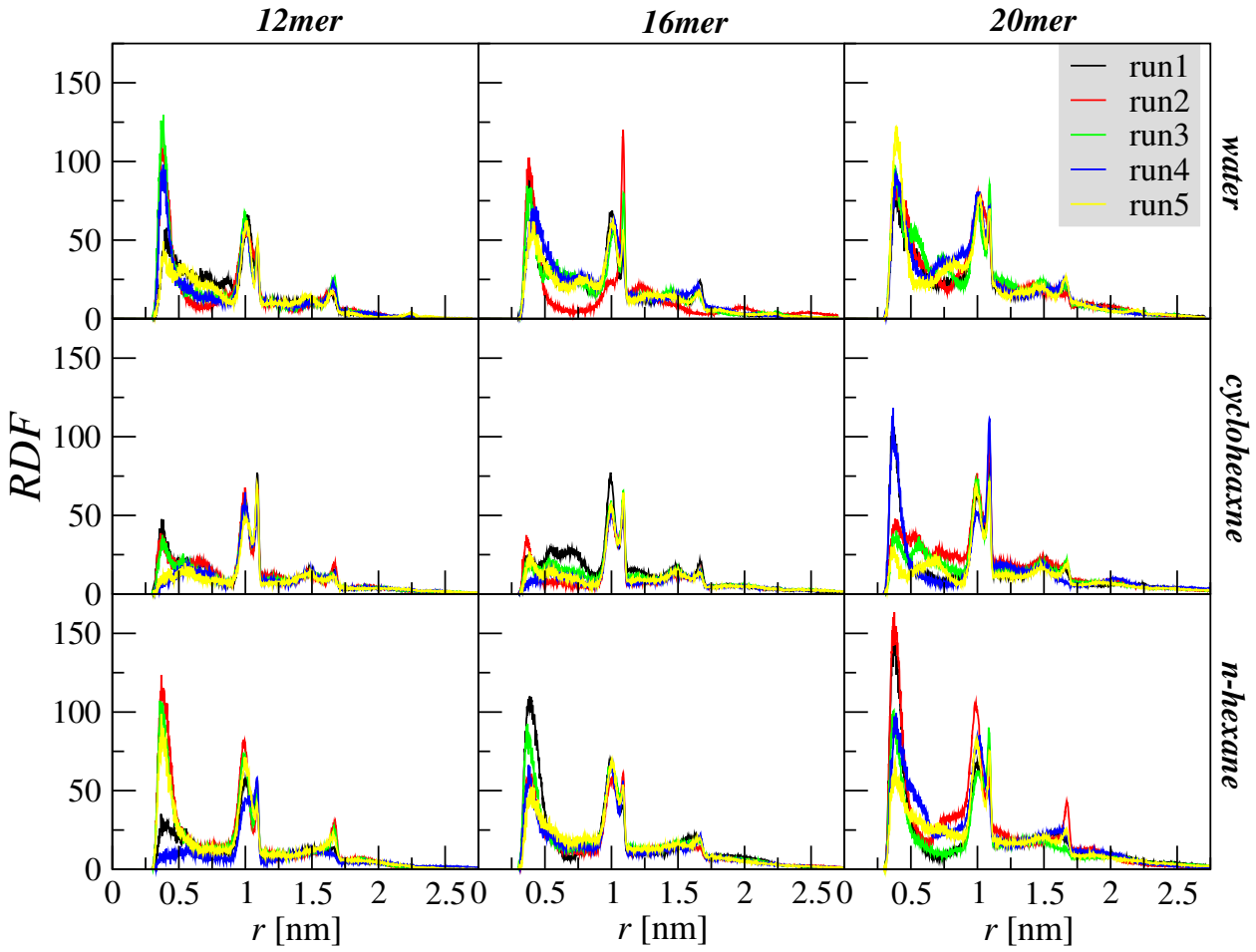

Figure SV: Intramolecular site-site pair radial distribution functions between carbon atoms of pPA methoxycarbonyl group in the three solvents H_2O (top), cyclohexane cC_6H_{12} (middle) and *n*-hexane (bottom) studied here. From left to right the changes in oligomer length *12mer*, *16mer* and *20mer* are respectively shown. Different colour correspond to individual runs performed.

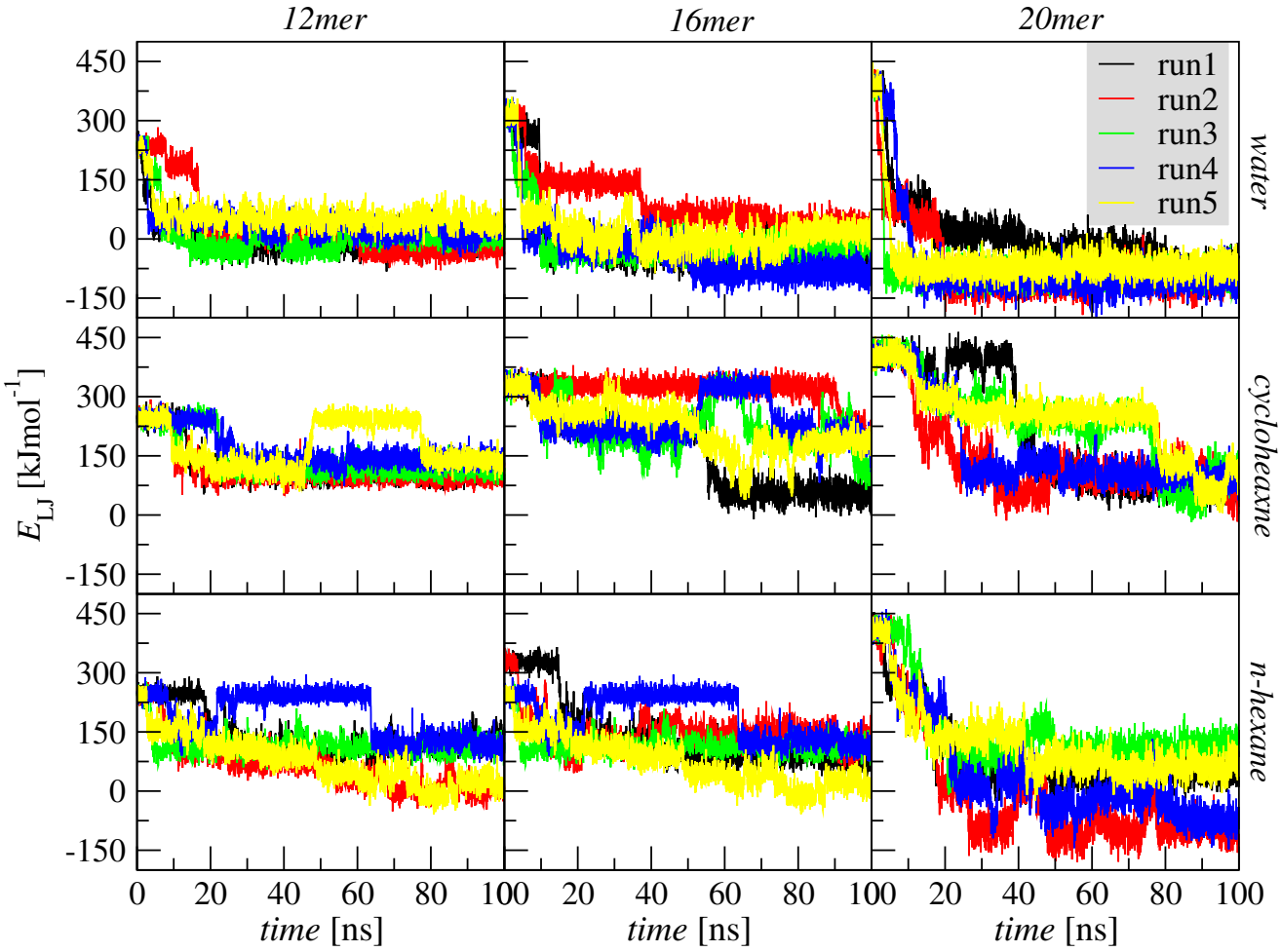

Figure SVI: Highlights of the self intramolecular Lenard-Jones non-covalent interaction energy along the simulation timescale. From top to bottom the changes recorded in water H_2O, cyclohexane cC_6H_{12}, and *n*-hexane nC_6H_{14}, respectively. From left to right the panels report on the oligomer's length-based results for *12mer*, *16mer*, and *20mer*, respectively. All the plots are on the same scale.

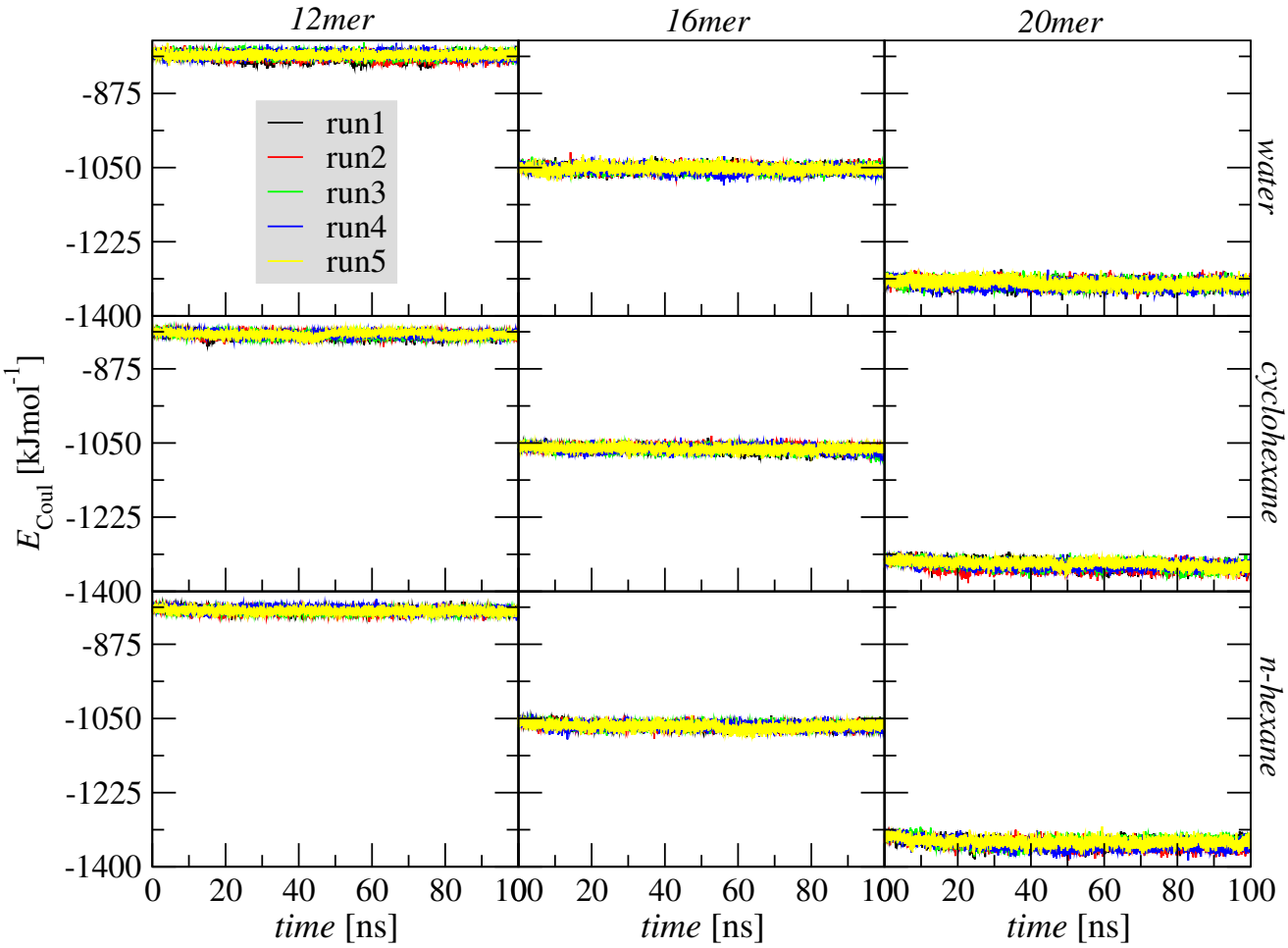

Figure SVII: Overview of the self intramolecular Coulombic non-covalent interaction energy along the simulation timescale. From top to bottom the changes recorded in water H_2O, cyclohexane cC_6H_{12}, and *n*-hexane nC_6H_{14}, respectively. From left to right the panels report on the oligomer's length-based results for *12mer*, *16mer*, and *20mer*, respectively. All the plots are on the same scale.

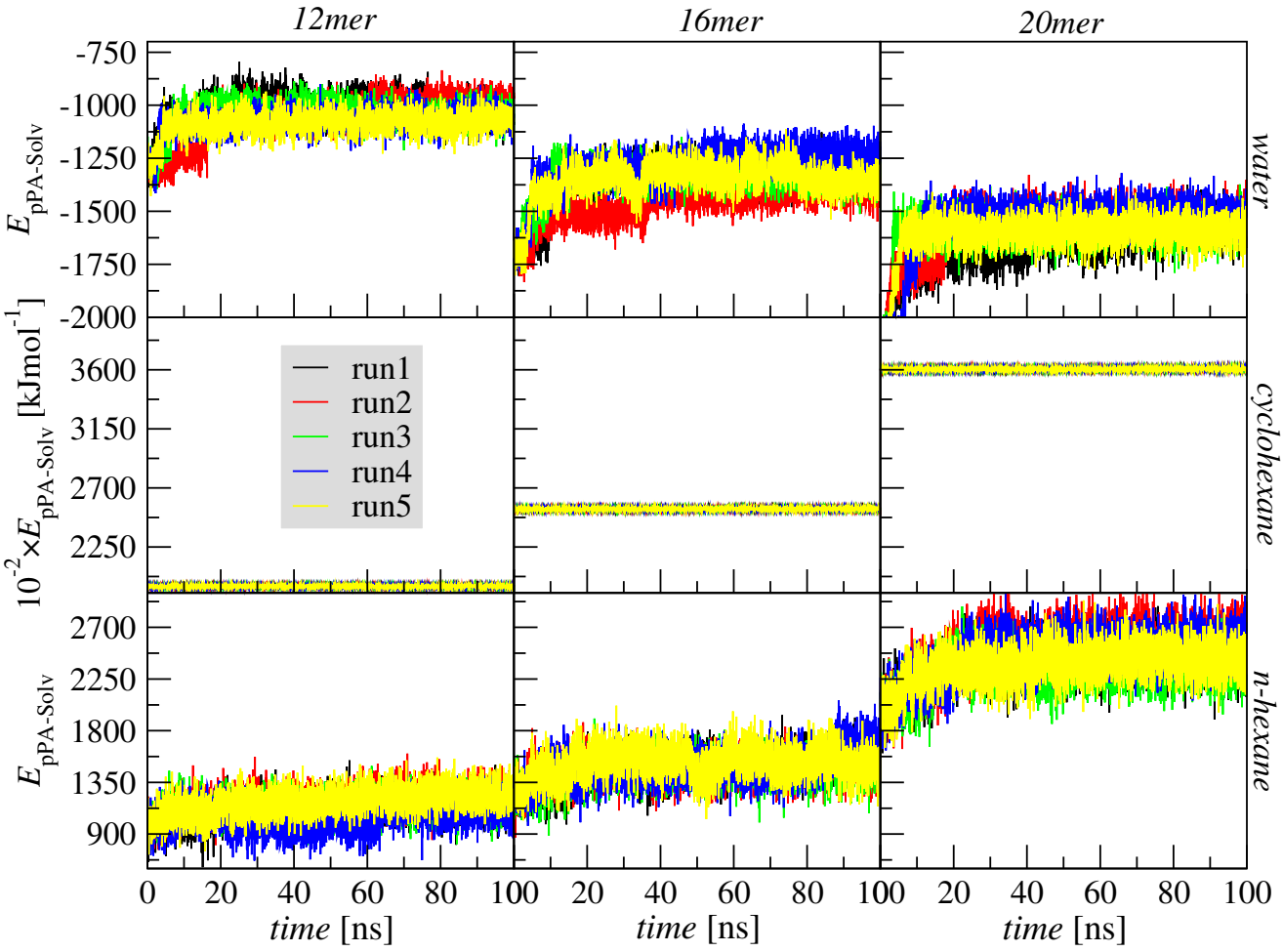

Figure SVIII: Panorama of the inter solute-solvent interaction energy changes with the simulation timescale. From top to bottom the changes computed in water H_2O, cyclohexane cC_6H_{12}, and *n*-hexane nC_6H_{14}, respectively. From left to right the views of the oligomer's length for *12mer*, *16mer*, and *20mer*, respectively. It should be noticed that each line is plotted on its own scale.

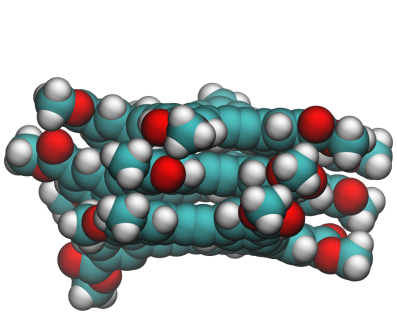

(a) Side view of the helical shape for *16mer*-pPA in cC_6H_{12}.

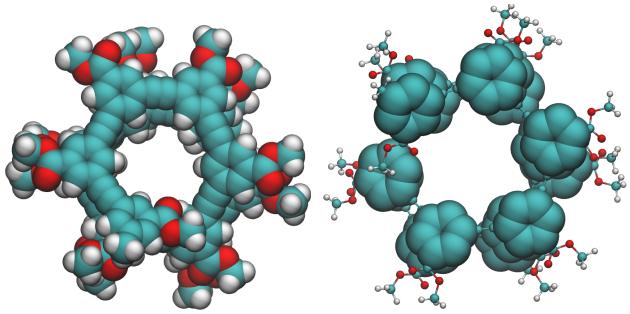

(b) Top views of the helical shape for *16mer*-pPA in cC_6H_{12}.

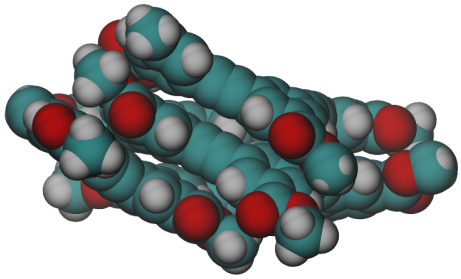

(c) Side view of the helical shape for *12mer*-pPA in H_2O.

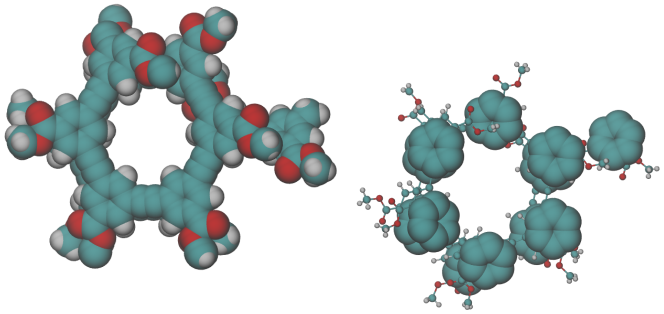

(d) Top views of the helical shape for *12mer*-pPA in H_2O.

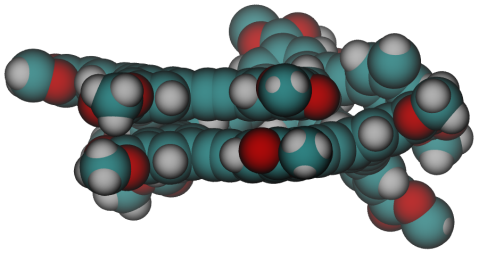

(e) Side view of the helical shape for *12mer*-pPA in H_2O.

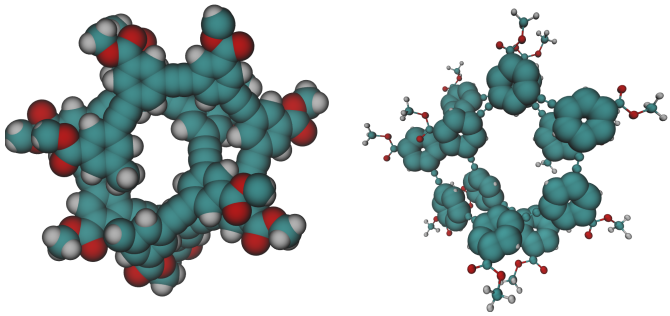

(f) Top views of the helical shape for *12mer*-pPA in H_2O.

Figure SIX: Close-up views of the best helical shapes obtained from the simulations of *12mer*-pPA in H_2O starting with two different conformations and of *16mer*-pPA in cC_6H_{12}. Different representations are displayed from side and top views to enable an in-dept view of the molecular arrangement and folded structures. In the latter top view, phenyl rings representing the core of each monomeric unit are explicitly shown.

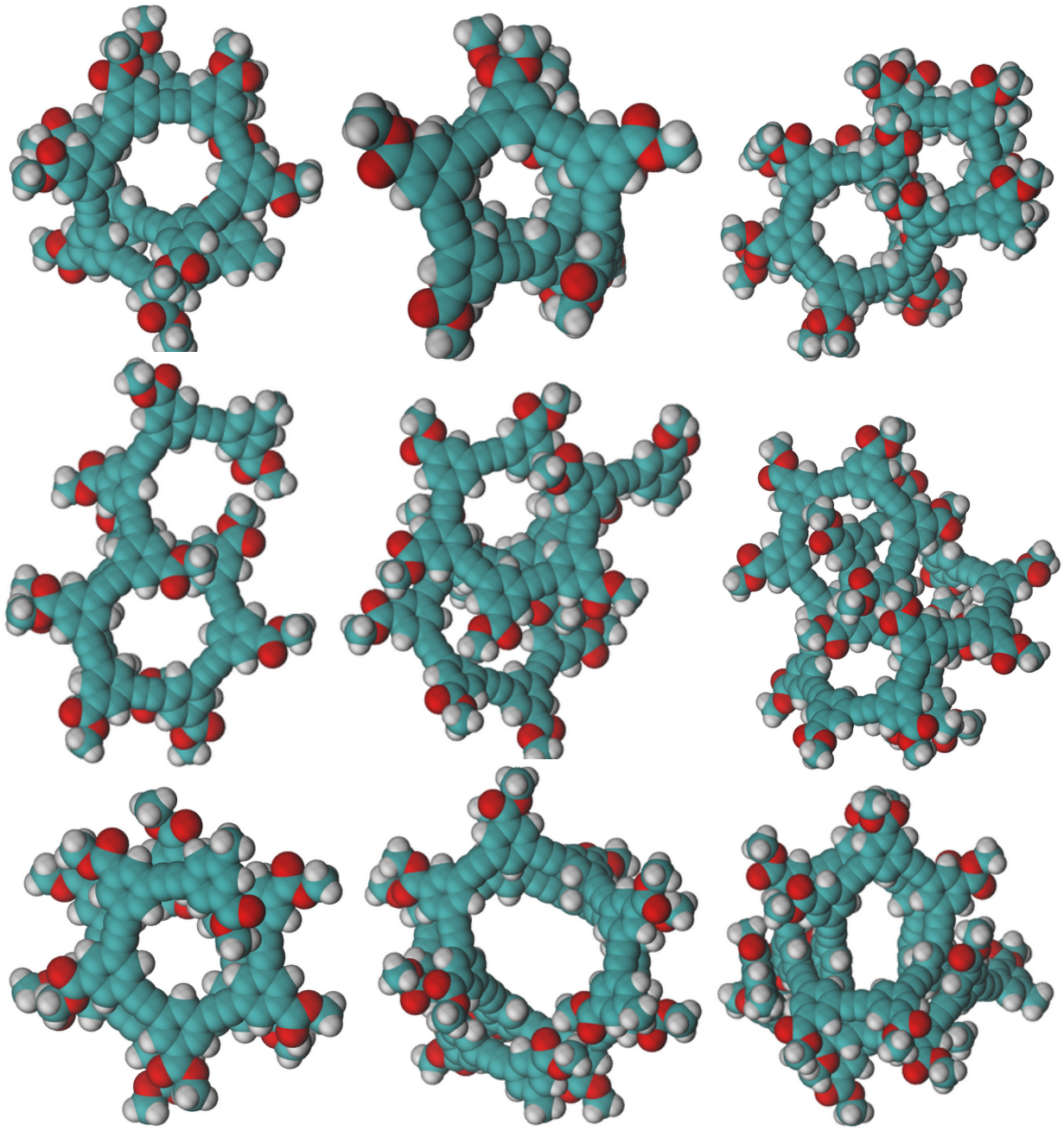

Figure SX: Representative structures of the most populated clusters found in the selected simulation trajectories. From top to bottom the structures identified in water H_2O, cyclohexane cC_6H_{12}, and *n*-hexane nC_6H_{14} are respectively shown. From left to right the snapshots of the *12mer*, *16mer* and *20mer* oligomers are presented, respectively.

FES-WATER

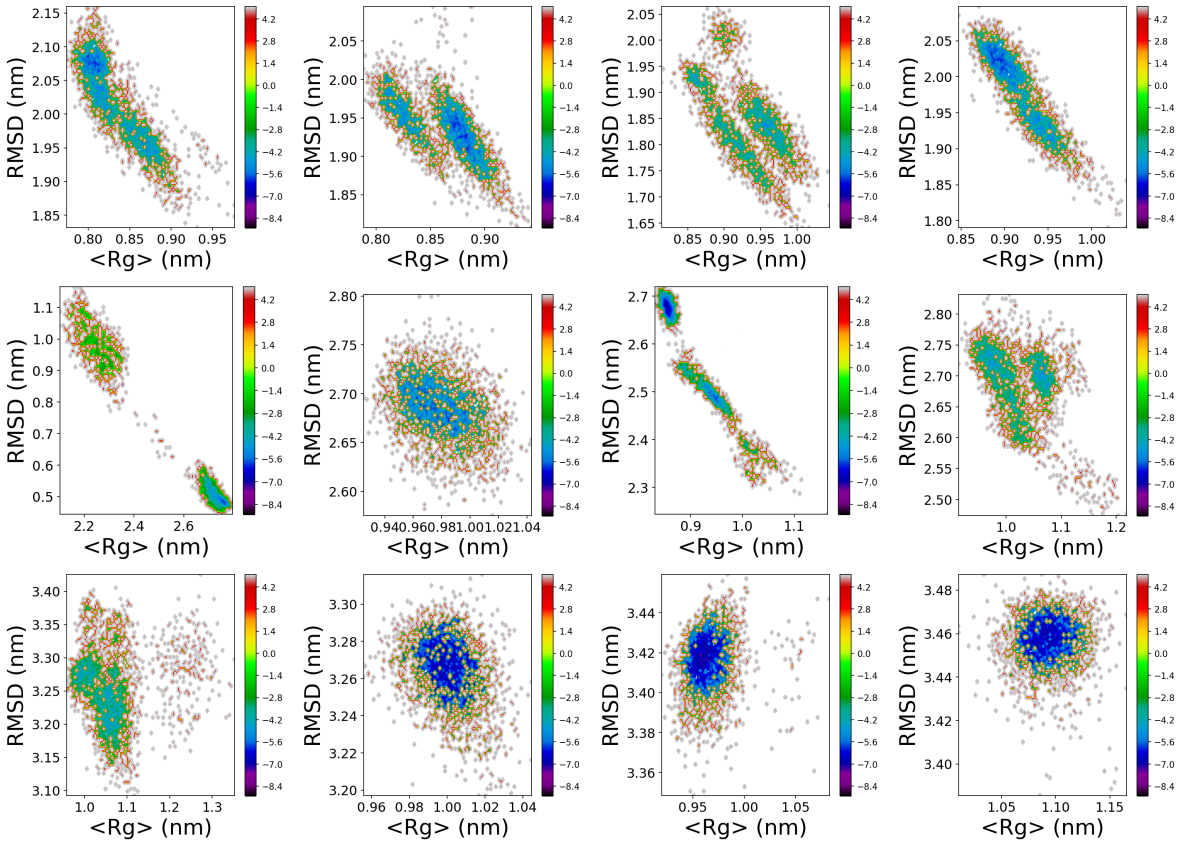

Figure SXI: Free Energy Surfaces (FES) of each of the oligomers used here in water H_2O. From top to bottom the FES for *12mer*, *16mer* and *20mer* oligomers, respectively. From left to right individual runs performed are displayed.

FES-CHEX

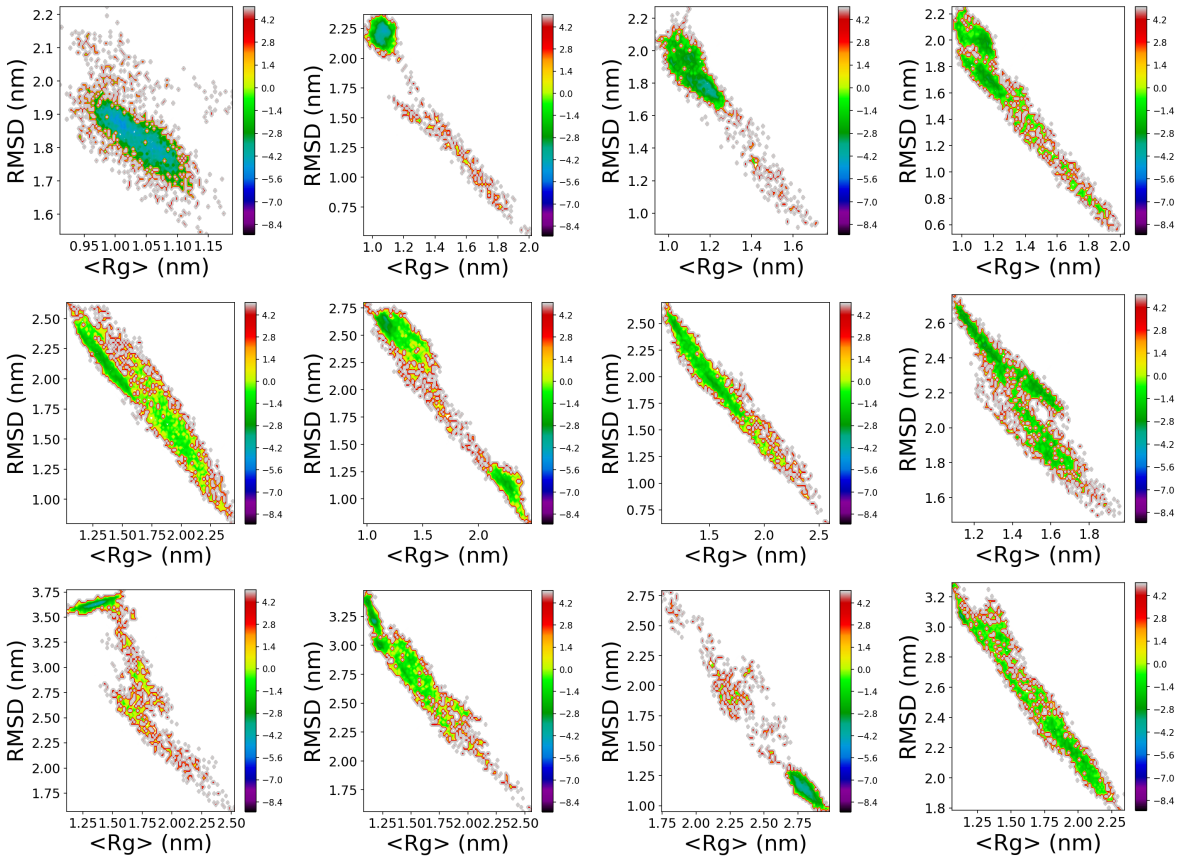

Figure SXII: Free Energy Surfaces (FES) of each of the oligomers used here in cyclohexane cC_6H_{12}. From top to bottom the FES for *12mer*, *16mer* and *20mer* oligomers, respectively. From left to right individual runs performed are displayed.

FES-HEX

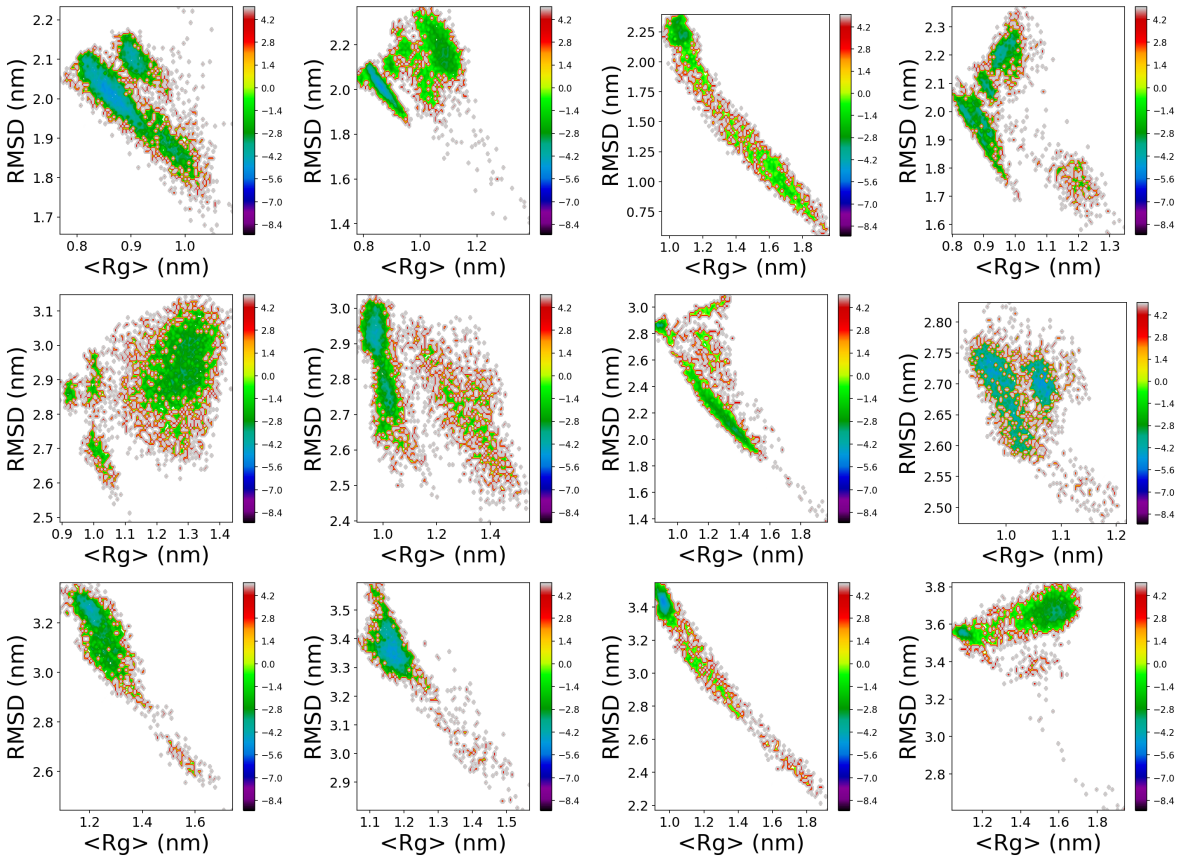

Figure SXIII: Free Energy Surfaces (FES) of each of the oligomers used here in *n*-hexane nC_6H_{14}. From top to bottom the FES for *12mer*, *16mer* and *20mer* oligomers, respectively. From left to right the individual runs performed are displayed.

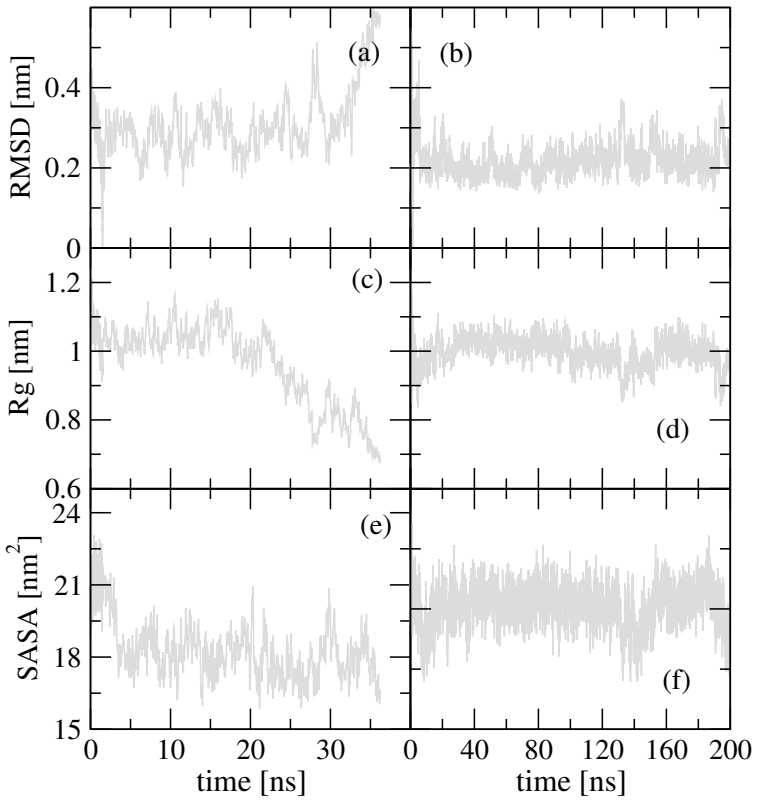

Figure SXIV: Conformational dynamics of unrestrained undecaphenylalanine in water (left) and in cyclohexane (right). Panels (a) and (b): root-mean-square-deviation (RMSD) from the initial state in water H_2O (a) and in cyclohexane cC_6H_{12} (b). Panels (c) and (d): radius of gyration R_g in water H_2O (c) and in cyclohexane cC_6H_{12} (d). Panels (e) and (f): the solvent accessible surface area (SASA) in water H_2O (e) and in cyclohexane cC_6H_{12} (f).

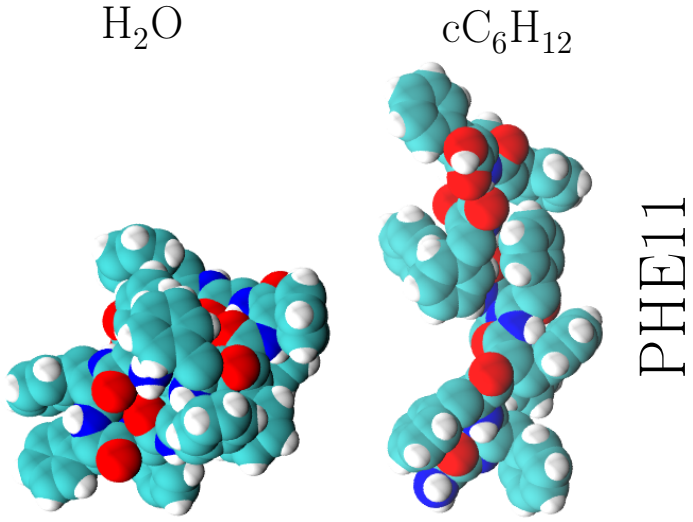

Figure SXV: Representative snapshots of the smallest R_g conformers i.e. the most collapsed conformations. On the left the structure obtained in water H_2O and on the right the one obtained in cyclohexane cC_6H_{12}.

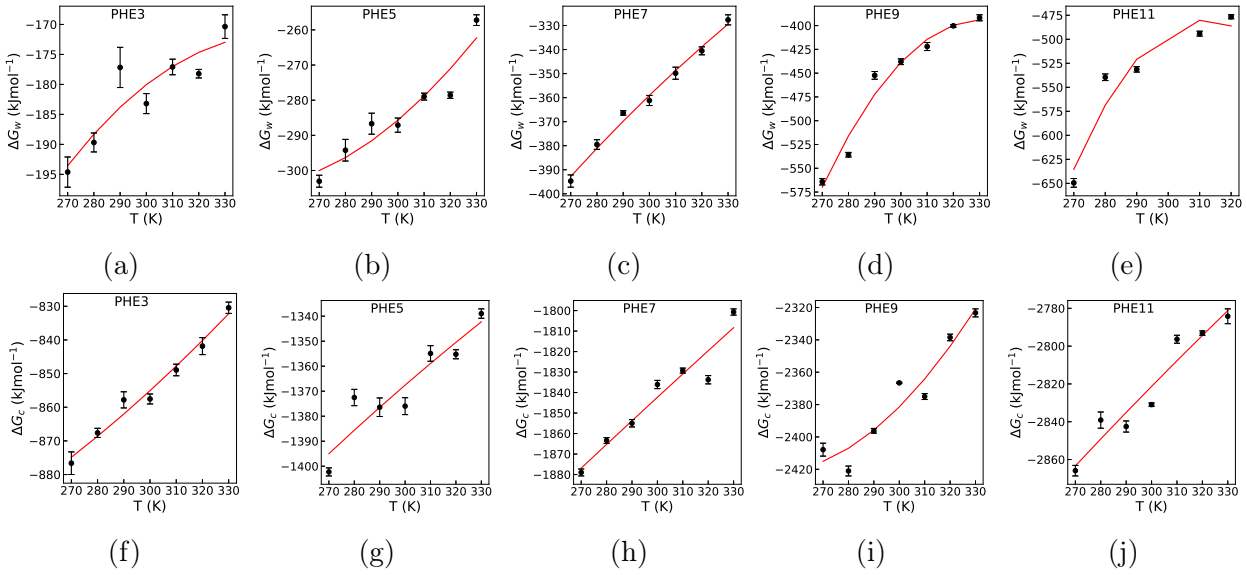

Figure SXVI: Temperature dependence of the solvation free energy ΔG_{solv} from gas to water H_2O (a $\cdots$ e) (top) and from gas to cyclohexane cC_6H_{12} (f$\cdots$j) (bottom) for the bio-polymer poly-phenylalanine oligomer polyPHE.

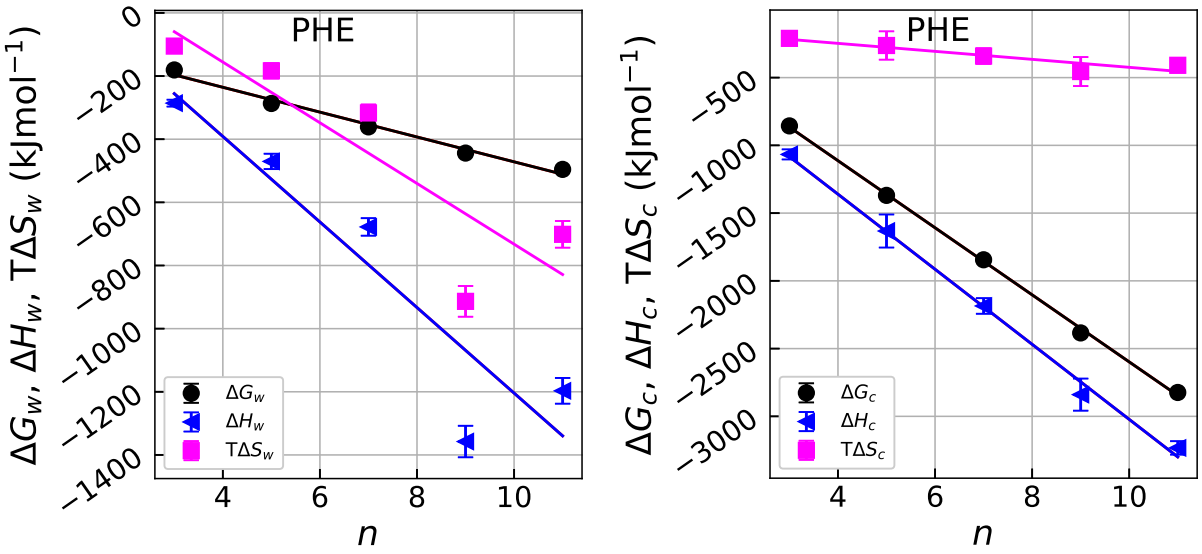

Figure SXVII: Solvation free energy, enthalpy, and entropy (ΔG, ΔH, $T\Delta S$) changes with the polymer chain length n in H_2O and in cyclohexane cC_6H_{12} at 25°C. The continuous lines connecting the points are the representative linear fitting. Negative ΔG and ΔH represent an energetic gain upon solvation, whereas a negative $T\Delta S$ represent an entropic loss, upon solvation.

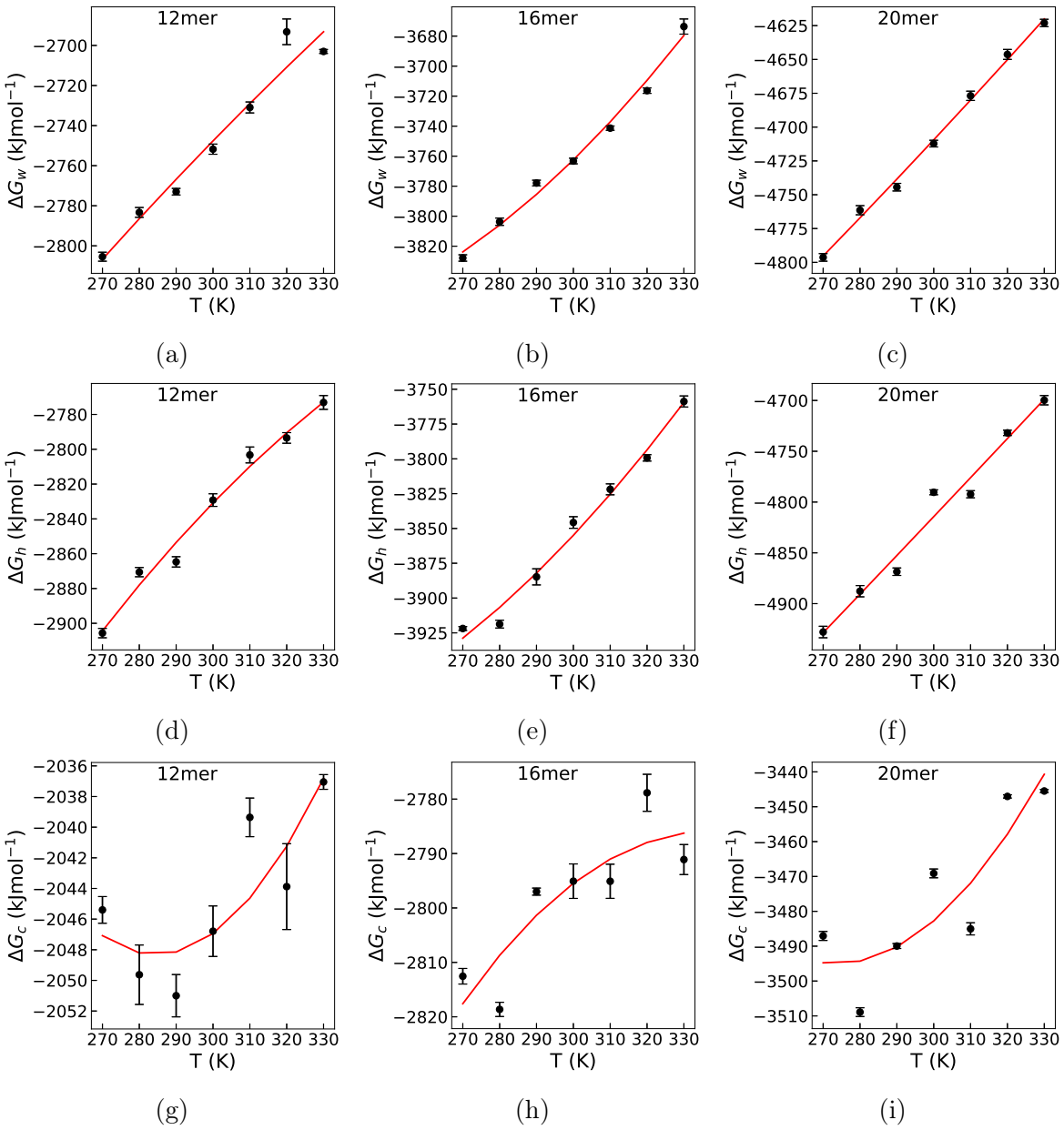

Figure SXVIII: Temperature dependence of the solvation free energy ΔG_{solv} from gas to water H_2O (a $\cdots$ c) (top), from gas to n-hexane nC_6H_{14} (d$\cdots$f) (middle) and from gas to cyclohexane cC_6H_{12} (g$\cdots$i) (bottom) for the synthetic polymer poly-phenylacetylene foldamer pPA.

Diffusion constants

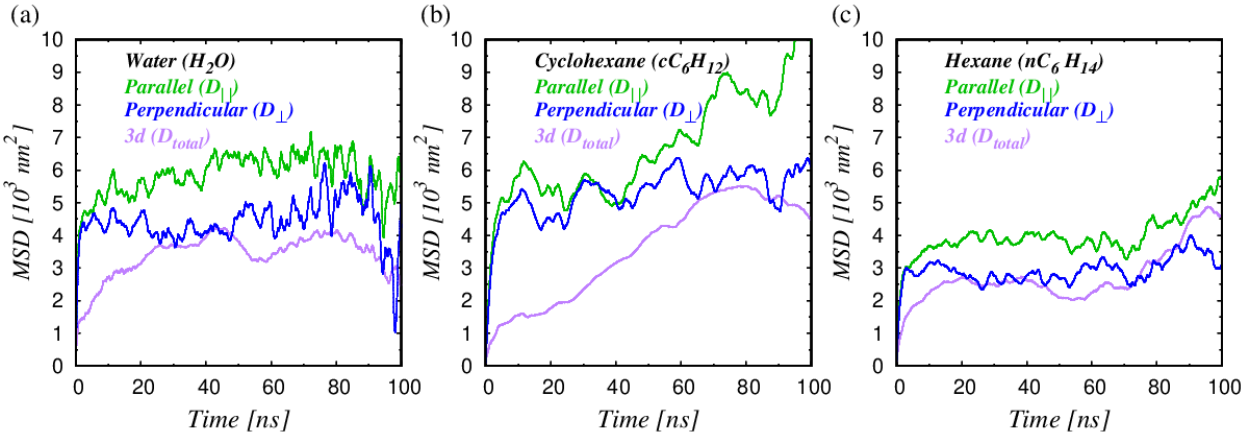

Figure SXIX: Mean square displacements (MSD) of the geometrical centers of 20 aromatic rings mid-points (GC) of pPA polymer (in units of $10^3 nm^2$) *vs* time (in ns) for three representative MD simulations of *20mers* solvated in water H_2O (Panel (a)), in cyclohexane cC_6H_{12} (Panel (b)), and in *n*-hexane nC_6H_{14} (Panel (c)). In each of the three panels the green lines represent the mean square displacement of GC along the direction parallel to the helical axis, namely $\langle \left(\mathbf{R}_{GC,||}(t) - \mathbf{R}_{GC,||}(0)\right)^2 \rangle = 2D_{||}t$; while the blue lines represent the MSD of GC along the direction perpendicular to the helical axis, $\langle \left(\mathbf{R}_{GC,\perp}(t) - \mathbf{R}_{GC,\perp}(0)\right)^2 \rangle = 4D_{\perp}t$. Finally the purple lines show the full MSD GC displacements in three dimensions, $\langle \left(\mathbf{R}_{GC}(t) - \mathbf{R}_{GC}(0)\right)^2 \rangle = 6D_{tot}t$. We note that diffusion is systematically larger along the direction parallel to helical axis with respect to the direction perpendicular to it.

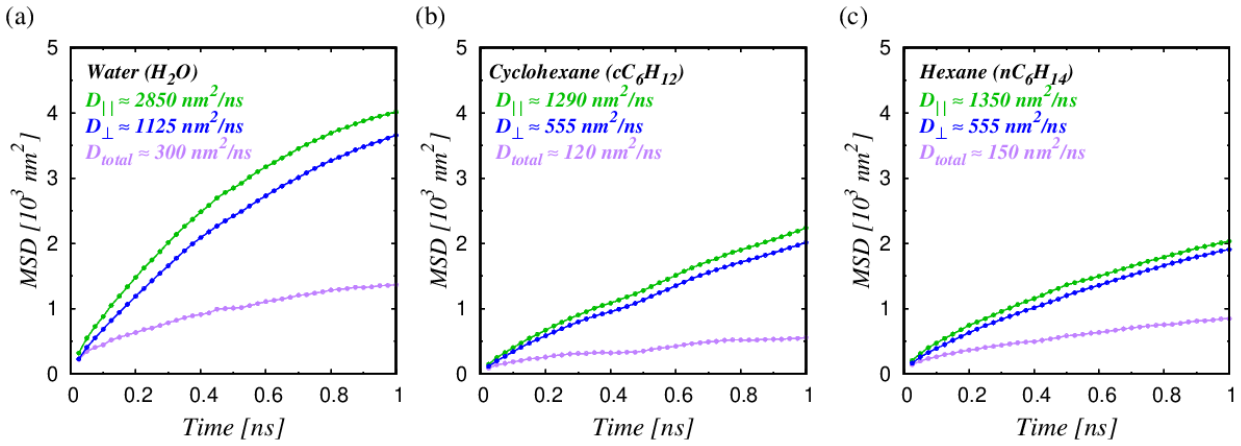

Figure SXX: Mean Square Displacements (MSD) of the geometrical centers of the 20 aromatic rings mid-points (GC) of *20mers* of pPA solvated in water (Panel (a)), in cyclohexane cC_6H_{12} (Panel (b)), and in *n*-hexane nC_6H_{14} (Panel (c)), for the initial stages of folding, similar to what is reported above in Figure SXIX. From the linear fits (up to $\sim 0.3ns$) we find the respective values of diffusion coefficients $D_{||}$, $D_{\perp}$, and D_{tot} in the three solvents. By comparing the values of the diffusion coefficients we conclude that diffusion in water is several times faster than in cyclohexane cC_6H_{12} and *n*-hexane nC_6H_{14}. Moreover, the diffusion coefficients in cyclohexane cC_6H_{12} and *n*-hexane nC_6H_{14} are on the other hand comparable to one another.